Giant cross sections for L changing in Rydberg-Rydberg collisions

S. Yoshida,[1] J. Burgdörfer,[1] G. Fields,[2] R. Brienza,[2] and F. B. Dunning[2]
[1]*Institute for Theoretical Physics, Vienna University of Technology Vienna, Austria, European Union*
[2]*Department of Physics and Astronomy, Rice University, Houston, Texas 77005-1892, USA*

(Received 12 March 2020; revised 18 June 2020; accepted 13 July 2020; published 4 August 2020)

State changing in thermal-energy collisions between strontium atoms in very-high-n, $n \approx 300$, $n\,^1F_3$ Rydberg states is studied. In collisions between Rydberg atoms, the dipole-dipole interaction generates an effective electric field at each atom, which triggers Stark precession and the evolution of their angular momenta, L. Such L-changing collisions are examined using both quantum and classical theory. The theoretical predictions are experimentally verified by monitoring the damping of quantum beats induced by the sudden application of a DC "pump" field. The present work shows that, due to the long-range nature of the interactions, the cross sections, σ, for L changing are considerably larger than the geometric collision cross section. For thermal collisions the cross section σ for $n\,^1F_3$ Rydberg states with $n \simeq 300$ is $\approx 8 \times 10^{-5}$ cm^2. Scaling rules derived in this paper predict that for cold collisions σ may increase by a further factor of 4.

DOI: 10.1103/PhysRevA.102.022805

I. INTRODUCTION

Interactions in many-body systems give rise to a rich variety of phenomena of fundamental importance in different fields of physics, among them in condensed matter physics including the creation of three-dimensional solitons, roton-maxon excitations, and supersolidity [1–3]. Many of these phenomena are amenable to study in ultracold gases but the effects of interactions depend strongly on their strengths. Several approaches for obtaining stronger interactions have been considered, including the use of systems such as ultracold polar molecules [4,5] or atoms with large magnetic moments [6]. Even stronger long-range interactions can be obtained by taking advantage of the large dipole moments of high-n Rydberg atoms, either through Rydberg dressing [2,7,8], in which a small admixture of Rydberg character is introduced into the atomic ground-state wave functions by illuminating them with radiation tuned near the transition to a Rydberg state, or by simply exciting a collection of Rydberg atoms themselves [9]. The strength of Rydberg-Rydberg interactions can be readily controlled by adjusting the atomic separations, by varying the principal quantum number, n, and by manipulating the atomic states [10–15]. Studies that exploit long-range Rydberg-Rydberg interactions, however, are complicated by collisions.

Collisions between Rydberg atoms can lead to a variety of outcomes [9,16–26]. Thermal energy collisions with impact parameters, b, smaller than or comparable to that associated with the geometric cross section, σ_g, i.e., with $b_g \lesssim (\sigma_g/\pi)^{1/2} \simeq 4n^2$, can lead to ionization if $b \lesssim 3n^2$ or n-changing processes if $b \lesssim 5n^2$ [26,27] (atomic units are used throughout unless otherwise noted). For larger impact parameters, the energy exchange that can occur between the collision partners is limited but is still sufficient to allow changes in the angular momentum, L, within a single n manifold. Such changes in L result from Stark precession [28,29] induced by the effective electric field, $F_{\rm eff} \sim \vec{d}_i/R^3$ associated with the dipole interaction $V_{\rm int} \sim \vec{d}_1 \cdot \vec{d}_2/R^3$ between the Rydberg atoms, where $\vec{d}_i$ is the dipole moment of the ith atom and R is the internuclear separation. Understanding L-changing processes is of interest not only for thermal-energy collisions but also in cold atom clouds where long interaction times can allow for a significant redistribution of angular momentum even if the interactions are weak.

In this paper, we present a joint theoretical-experimental study of L changing in Rydberg-Rydberg collisions. We perform quantum calculations for low-n ($n \simeq 30$) and classical trajectory Monte Carlo (CTMC) simulations for n up to $\simeq 300$, thereby probing classical-quantum correspondence and scaling invariance. True quantum effects manifest themselves in terms of violation of such dilatation symmetry. These theoretical predictions are tested experimentally by creating a tightly collimated string of strontium Rydberg atoms in a thermal atomic beam ($T \simeq 830$ K) with approximately equal initial separations of ≈ 150–$200\,\mu$m but a distribution of velocities which leads to Rydberg-Rydberg collisions. The final collision products are analyzed by a pump-probe technique. The "pump" pulse is provided by sudden application of a field step with a short rise time $t_R \ll T_n$, where T_n is the classical orbital period, ≈ 4 ns at $n \approx 300$. This creates a Stark wave packet whose time evolution is sensitive to the n and L distributions [30] that result from the Rydberg-Rydberg collisions. The evolution of this wave packet is monitored by application of a 600-ps-long "probe" pulse that ionizes a (time-dependent) fraction of the Rydberg atoms. In Sec. II, the experimental setup used in the current study is briefly introduced. In Sec. III, the time evolution of the electronic state during a collision of two Rydberg atoms is analyzed. The methods employed to calculate the L- and n-changing cross sections using both quantum and the classical theory [26] are described in Sec. IV and their predictions are compared. The comparison of these microscopic predictions with the experiment requires the mesoscopic simulation [31] of excitation

and collisions of an ensemble of Rydberg atoms in a thermal beam within the excitation volume of the lasers involved. It furthermore requires the simulation of the probe protocol [30], again on the atomic scale, with which the collisional state changes of Rydberg atoms are monitored. Both of these simulation methods are briefly discussed in Sec. V. In Sec. VI, we present the results where we find good agreement between experimental observations and theoretical predictions. Our results point to remarkably large cross sections for L changing in collisions between strontium $5s297f\ n\ ^1F_3$ Rydberg atoms of the order of $\approx 8 \times 10^{-5}$ cm^2, much larger than the "hard-sphere" collision cross section, $4\pi R^2$, where $R \sim 2n^2$ is the maximum extent of the electron charge cloud. Furthermore, application of the scaling relations established in this paper suggests that the cross section should increase even further for cold collisions down to temperatures of the order of $T \lesssim 70$ K.

II. EXPERIMENTAL APPROACH

In the present work, ground-state strontium atoms contained in a collimated beam produced using a heated (≈ 830 K) oven are excited to Rydberg states through laser-induced multiphoton excitation using crossed focused laser beams that define a small excitation volume whose linear dimensions, $\approx$ 50–70 μm, are less than the blockade radius, R_b, ≈ 100 μm at $n \approx 300$ [32]. Excitation of a Rydberg atom in this volume suppresses further excitation until the atom has typically traveled one blockade radius in the beam direction which, given the mean velocity of atoms in the beam, $\bar{v} \approx 4 \times 10^2$ m/s, typically requires ≈ 250 ns. (However, there is a small but finite probability to excite a Rydberg atom within the blockade radius [32]). Thus, when using high laser powers such that excitation of an additional Rydberg atom occurs quickly once a previously excited Rydberg atom has moved more than a blockade radius, a string of Rydberg atoms can be produced with approximately equal initial separations but a distribution of initial velocities. Laser pulse widths of a few microseconds are employed, sufficient to allow production of multiple Rydberg atoms.

The present apparatus is shown in Fig. 1 and is described in detail elsewhere [26]. Briefly, ^{88}Sr $n\ ^1F_3$ Rydberg atoms are created in near-zero ($\lesssim 50$ μV cm^{-1}) electric field at the center of an interaction region defined by three pairs of copper electrodes. The three-photon excitation scheme employed $5s^2\ ^1S_0 \rightarrow 5s5p\ ^1P_1 \rightarrow 5s5d\ ^1D_2 \rightarrow 5snf\ ^1F_3$ is illustrated in the inset in Fig. 1. The required radiation is provided by diode laser systems whose wavelengths are stabilized using Fabry-Perot transfer cavities that are locked to a 689-nm "master" laser that is itself locked to the $5s^2\ ^1S_0 \rightarrow 5s5p\ ^3P_1$ transition in ^{88}Sr. (Three-photon excitation has the advantage that sizable laser powers (>1 W) are available to drive the final transition to the Rydberg state). The crossed 767- and 893-nm beams are focused to $1/e^2$ diameters of ≈ 50 and ≈ 70 μm, respectively, resulting in a strongly localized excitation volume of $\approx 10^{-7}$ cm^3 that typically contains many tens of ground-state atoms.

Measurements are conducted in a pulsed mode. The output of the 461-nm laser, which is not focused, is chopped into a series of pulses with a pulse repetition frequency of

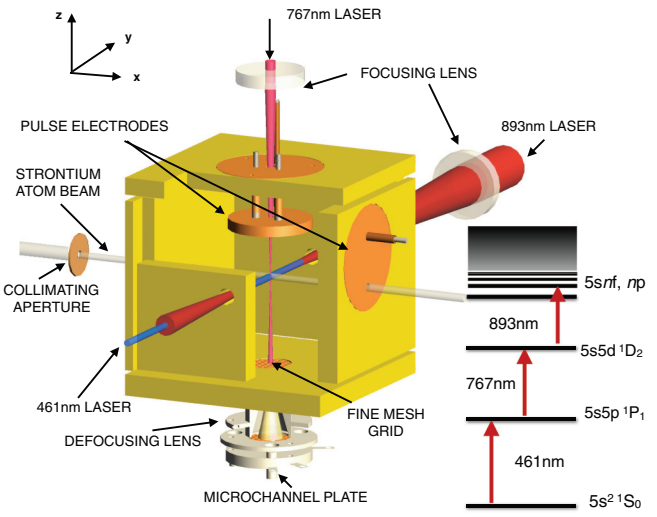

FIG. 1. Schematic diagram of the apparatus. The inset shows the three-photon excitation scheme employed.

$\approx$ 5–10 kHz using an acousto-optic modulator. (The other laser beams remain on at all times). Immediately following excitation the effects of n, L changing during the laser pulse are monitored by sudden application of a voltage step (rise time ≈ 300 ps) to the upper pulse electrode which generates a "pump" electric field, F_{pump}, and creates a Stark wave packet. The time evolution of the wave packet is examined using a 600-ps-long unidirectional probe pulse (that is also applied to the upper pulse electrode) and varying the time delay, t_{probe}, between application of the pump and probe fields. The range of delay times over which measurements are made is short, $\lesssim 300$ ns, and any effects of collisions during this interval are small. The number of surviving Rydberg atoms is determined following the end of the probe pulse by selective field ionization (SFI), which is accomplished by generating a slowly increasing (rise time ≈ 3 μs) electric field in the experimental volume by applying a linearly increasing voltage ramp to the lower electrode. The number of electrons so produced is determined by directing them through two fine-mesh grids to a dual-microchannel-plate (MCP) detector. The electron detection efficiency of the microchannel plates could not be determined directly but is estimated to be 0.5 which, when corrected for transmission through the grids, results in an overall detection efficiency, η, of ≈ 0.3 [26]. Survival probabilities were obtained by comparing the SFI signals observed with and without the pump and probe fields applied.

III. DESCRIPTION OF RYDBERG-RYDBERG COLLISIONS

In a hot strontium atomic beam ($k_BT \approx 2.5 \times 10^{-3}$ a.u. for $T \approx 830$ K) and the reduced mass $\mu \approx 8.0 \times 10^4$ a.u., the thermal de Broglie wave length,

$$\lambda_d = \frac{2\pi}{\sqrt{2\mu k_B T}}, \tag{1}$$

is negligibly small ($\lambda_d \simeq 0.31$ a.u.) compared to the size of the interacting Rydberg atoms which have average radii $\langle r \rangle_n \sim (3/2)n^2$, i.e., $\lambda_d / \langle r \rangle_n \ll 1$. Therefore, the translational motion of the ionic cores during a collision is described throughout

this paper classically. Moreover, the collision energy $E_{\rm coll}$ is, typically, much larger than the potential energy of the interacting Rydberg atoms. In this limit, the relative motion of the ionic cores can be described not only classically but the curved trajectories can be approximated by straight-line trajectories

$$\vec{R}(t) = \vec{R}_1(t) - \vec{R}_2(t) = \vec{b} + \vec{v}_{\rm coll} t \tag{2}$$

with $\vec{b}$ being the impact parameter vector and $E_{\rm coll} = (1/2)\mu v_{\rm coll}^2$. The applicability of this straight-line impact parameter (IP) approximation [33] for $n \approx 300$ and a Rydberg atom density $\approx 10^7$ cm^3) is restricted to collision energies above 10^{-8} a.u. which corresponds to thermal gases with T above $\simeq 3$ mK.

Within the IP approximation, the motion of the ionic cores is fixed and provides time-dependent fields controlling the dynamics of the effective two-electron system of two colliding atoms governed by the Hamiltonian

$$H = H_0 + V_{\rm int}(t), \tag{3}$$

where

$$H_0 = \sum_{i=1}^{2} \left[\frac{p_i^2}{2} + V_c(r_i) \right] \tag{4}$$

and

$$V_{\rm int}(t) = -\frac{1}{|\vec{r}_1 + \vec{R}(t)|} - \frac{1}{|\vec{r}_2 - \vec{R}(t)|} + \frac{1}{|\vec{r}_1 - \vec{r}_2 + \vec{R}(t)|} + \frac{1}{R(t)}. \tag{5}$$

Each atom is separately described by a single active electron model and $V_c(r)$ represents the model core-ion potential seen by the Rydberg electron. For the electronic dynamics, we will perform both quantum and classical simulations. In the quantum simulations, the intraatomic interaction with the core will be parameterized by the quantum defects. Correspondingly, in the classical simulation we employ for the potential the explicit form

$$V_c(r) = -\frac{1}{r}\left[1 + (Z-1)e^{-a_1 r} + a_2 e^{-a_3 r} - \frac{\alpha_{\rm cp}}{2r^4}(1 - e^{-(r/r_c)^6}) \right], \tag{6}$$

where $Z = 38$ is the atomic number. The parameters $a_1 = 3.3$, $a_2 = 6.0$, $a_3 = 1.3$, and $\alpha_{\rm cp} = 5.3$ are optimized to reproduce the measured quantum defects. In the present study, our focus is on the dynamics of distant collisions with very large impact parameters b. Therefore, the Rydberg-Rydberg interaction potential $V_{\rm int}(r)$ reduces to purely Coulombic two-center interactions [Eq. (5)].

Thermal collisions between Rydberg atoms with impact parameters comparable to the size of the Rydberg charge cloud ($b \lesssim 3n^2$) can result in the destruction of Rydberg atoms by nonadiabatic transitions to the continuum, i.e., ionization [27]. However, previous studies [26] using a similar experimental arrangement showed that, for experimental conditions such as those employed here, the probability of collisional ionization is small, at most a few percent. In the present experiments, the great majority of Rydberg atoms experience only distant collisions and undergo state-changing processes without ionization.

For collisions with $R \gg \langle r \rangle_n$, the leading-order term of the Taylor expansion of the interaction potential [Eq. (5)] gives the dipole-dipole interaction

$$V_{\rm int}(t) \xrightarrow{R \gg \langle r \rangle_n} V_{\rm dd}(t) \simeq \frac{\vec{r}_1 \cdot \vec{r}_2}{R(t)^3} - \frac{3[\vec{r}_1 \cdot \vec{R}(t)][\vec{r}_2 \cdot \vec{R}(t)]}{R(t)^5}. \tag{7}$$

Accordingly, the collision process can be viewed as a perturbation of Rydberg atom i by an effective field induced by atom j which is of the order of $F_{\rm eff}(t) \sim \vec{r}_j / R(t)^3$. In consequence, L-changing collisions can be interpreted as dynamical Stark mixing by the time-dependent electric field produced by atom j as it passes by atom i. As will be shown below, this simplified model leads to an estimate for the L-changing cross section.

Our quantum simulations of the electronic dynamics in Rydberg-Rydberg collisions proceed by solving the time-dependent Schrödinger equation (TDSE) described by the Hamiltonian [Eq. (3)] with the interaction $V_{\rm int} \simeq V_{\rm dd}$ approximated by the dipole-dipole interaction [Eq. (7)]. The matrix elements of H_0 are evaluated using quantum defects extrapolated from the measured data [34] representing the electron-core interaction $V_c(r)$. By solving this Hamiltonian nonperturbatively, the van der Waals interaction, which appears to second order in $V_{\rm dd}$, is fully accounted for. Here, we focus on large impact parameters for which collisions populate a broad distribution of L states. In contrast, collisions populate only a narrow band of n levels centered near the initial n level, $n_{\rm ini} \approx 300$. Thus, the TDSE

$$i\partial_t |\Psi(t)\rangle = H|\Psi(t)\rangle \tag{8}$$

can be numerically solved as time-dependent coupled channels (TDCC) equations [35] using the basis states of the two noninteracting Rydberg atoms labeled as $|n_1, L_1, M_1; n_2, L_2, M_2\rangle$, with a limited number of n levels ($n_{\rm ini} - \Delta n < n_{1,2} < n_{\rm ini} + \Delta n$) and all L and M states included. In practice, for $n_{\rm ini} \approx 300$ and $\Delta n = 1$, more than 20 billion basis states (even after taking into account the symmetry of $V_{\rm dd}$) would be required. To reduce this number to a workable size, calculations are only performed for $n_{\rm ini} \lesssim 35$, which reduces the basis size to less than 4 million. The eigenenergies of the unperturbed Hamiltonian H_0 are determined by the quantum defects and the dipole matrix elements for $V_{\rm dd}$ are evaluated in the large n-limit [36], assuming that the quantum defects are n independent. (We note that due to the interaction between the two valence electrons the quantum defects for strontium show weak n dependences for lower n states [34,37,38]. By neglecting this weak n dependence, the extrapolation of the quantum results to $n \approx 300$, as discussed below, becomes straightforward). We initially take both atoms to be in the Rydberg state $(n, L, M) = (n_{\rm ini}, 3, 0)$, to be far apart with a separation $R_\parallel = 20 n_{\rm ini}^2$ in the direction parallel to $\vec{v}_{\rm coll}$, and have impact parameter b. ($\vec{v}_{\rm coll}$ defines the quantization axis). The Schrödinger equation is integrated by the iterative Lanczos method [39,40] and the L and n distributions after the collision evaluated. Cross sections can be obtained

from the resulting probability distributions $P_{nL}(b)$ via

$$\sigma_{nL} = 2\pi \int_0^\infty dbbP_{nL}(b), \tag{9}$$

where we have used the rotational symmetry about the velocity $\vec{v}_{\rm coll}$ axis. For the comparison with the measured data presented later, we perform a rotational average over all M (i.e., an isotropic distribution in the orientation of $\vec{L}$). As a test of classical-quantum correspondence for lower $n \simeq 20$–40 and for applications to very high $n(\gtrsim 100)$ for which full quantum simulations are no longer feasible, we perform in parallel classical trajectory Monte Carlo (CTMC) simulations. Here, the classical approximation refers to the electronic degree of freedom. Accordingly, the quantum wave function of the initial state is represented by an ensemble of classical electrons taken to be restricted microcanonical ensembles [41,42]. The time evolution of the ensemble is calculated by solving the Liouville equation for the Hamiltonian [Eqs. (3)–(6)]. Upon conclusion of the collision, the classical phase space distributions are binned according to their energy and angular momenta from which probability distributions $P_{nLM}(b)$ can be deduced. Within the CTMC approximation, unlike for the full quantum simulation, it is straightforward to employ the full interaction potential $V_{\rm int}$ [Eq. (5)] rather than its limiting case $V_{\rm dd}$ [Eq. (7)] and also to include curved rather than straight-line trajectories, thereby allowing detailed tests of those approximations. For the range of parameters used in the current study, these tests confirm the validity of the straight-line IP approximation and the usage of $V_{\rm dd}$.

The results of quantum calculations are extrapolated to high n by taking advantage of the invariance of the pure Coulomb problem. To this end, the results are discussed using the scaled phase-space variables, denoted by subscripts 0,

$$b = n_{\rm ini}^2 b_0, \quad t = n_{\rm ini}^3 t_0, \quad v_{\rm coll} = v_{\rm coll,0}/n_{\rm ini},$$
$$F_{\rm eff} = F_{\rm eff,0}/n_{\rm ini}^4. \tag{10}$$

Since the temperature T of the atomic beam is approximately proportional to collision energy, i.e., $T \propto (1/2)\mu v_{\rm coll}^2$, the temperature scales as $T = T_0/n_{\rm ini}^2$.

IV. CLASSICAL-QUANTUM CORRESPONDENCE FOR DYNAMICAL L MIXING

The time evolution of the L distribution during a Rydberg-Rydberg collision is shown in Fig. 2(a) and is calculated for the scaled impact parameter $b_0 = 5$ and collision velocity $v_{\rm coll,0} = 0.025$, which represent typical values for the current experimental conditions. (Note that the maximum scaled impact parameter for a "hard-sphere" collision, for which the two charge clouds have substantial overlap, is $b_0 \simeq 3$). The trajectory is started at $R_{\parallel,0} = v_{\rm coll,0}|t_0|$ with $t_0 = -800$. When the scaled interatomic distance $R_0(t_0) = \sqrt{b_0^2 + (v_0 t_0)^2}$ decreases below $R_0 \simeq 9$, at $t_0 > -300$, the angular momentum L starts to evolve due to Stark precession. This evolution becomes more rapid as the two atoms move toward their distance of closest approach at $t_0 = 0$ (indicated by the arrow). Since $\vec{F}_{\rm eff}$ varies in both magnitude and direction during the collision, Stark precession leads to creation of states with a broad distribution of L encompassing the entire range 0 to

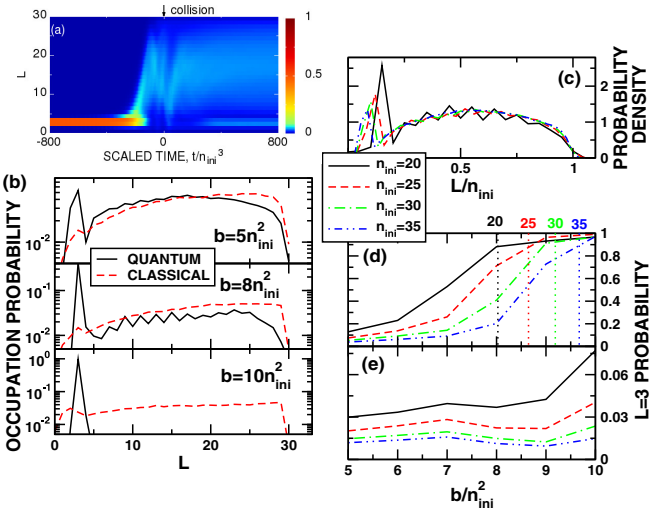

FIG. 2. (a) Time evolution of the L distribution during a collision of two $L = 3$ Rydberg atoms ($n_{\rm ini} = 30$) for $b = 5n_{\rm ini}^2$ and $v_{\rm coll} = 0.025/n_{\rm ini}$. The calculation is performed by solving the Schrödinger equation. The time of closest approach at $t = 0$ is indicated by the arrow. (b) Final L distribution following collisions with different impact parameters as indicated. The results of classical simulations are also shown (dashed line). (c) Quantum-mechanically-calculated L distributions following collisions involving atoms with the values of $n_{\rm ini}$ indicated plotted as a function of scaled angular momentum. (d) Quantum and (e) classical calculations of the probability that an atom remain in the initial $L = 3$ state after collision as a function of scaled impact parameter for several values of $n_{\rm ini}$. The vertical dotted lines in panel (d) indicate the threshold $b_{\rm qd,0} = [9n_{\rm ini}/(4\delta_F)]^{1/3}$ above which Stark precession is suppressed (see text).

$n - 1$. However, Stark precession is dramatically suppressed by increasing the impact parameter. Final L distributions at $t_0 = 800$ are shown in Fig. 2(b) for several impact parameters. As the scaled impact parameter becomes larger than the threshold value, $b_{\rm qd,0}(L) \simeq 9$, where the influence of the quantum defect δ_L starts to dominate, the probability for creation of high-L states decreases and the probability that an atom will remain in its initial $L = 3$ state grows. Indeed, when $b_0 = 10$, L evolution is frozen and nearly no L changing occurs. This threshold effect is due to the finite-size quantum defect of the F state ($\delta_F = 0.087$). For larger b_0, the nonadiabatic coupling to the degenerate manifold of high-L states is too weak to overcome the energy gap to the nearby quasihydrogenic manifold. Since this excitation gap is a true quantum effect it is not present in the classical dynamics and, as shown in Fig. 2(b), the CTMC simulations start to deviate from the quantum calculations. For smaller values of b_0, good agreement between the classical and quantum result is found, except for the local maximum at $L = 3$, the state with sizable quantum defect [Fig. 2(b)]. For $b_0 < b_{\rm qd,0}(L)$, the L distribution calculated from the Schrödinger equation is approximately scaling invariant [Fig. 2(c)]. The probability densities, $P_{nL}(b)$, expressed as a function of the scaled angular momentum $L_0 = L/n_{\rm ini}$ for different values of $n_{\rm ini}$ become nearly indistinguishable. Only the peak near $L_0 = 3/n_{\rm ini}$ is $n_{\rm ini}$ dependent and decreases with increasing $n_{\rm ini}$. Since the major difference between the classical and quantum simulations is

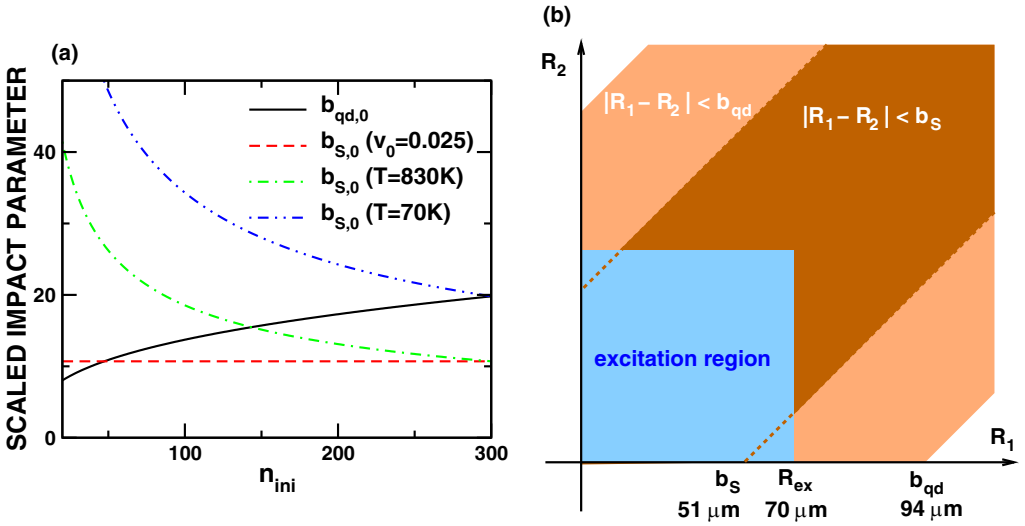

FIG. 3. (a) Threshold values in impact parameter b_0 as a function of $n_{\rm ini}$: $b_{\rm qd,0}$ (solid line), $b_{S,0}$ with a fixed $v_{\rm coll,0} = 0.025$ (dashed lined), and $b_{S,0}$ with a fixed temperature at $T = 830$ K (dash-dotted line) and at $T = 70$ K (double-dot-dashed line). For a fixed temperature, the scaled velocity scales as $v_{\rm coll,0} \propto n_{\rm ini}\sqrt{T}$. (b) Schematic illustration for $b_{\rm qd}$ and b_S of strontium $n = 300$ $^1F_3$ Rydberg atoms with $v_{\rm coll,0} = 0.025$ in the plane of (R_1, R_2) (i.e., the positions of two Rydberg atoms). For visualization, the excitation region of each atom is reduced to one dimension and $R_{\rm ex}$ is set to the larger one of the linear dimensions of the atomic excitation region ($50 \times 70\,\mu$m in diameter). The regions $|R_1 - R_2| < b_S$ (dark brown) and $|R_1 - R_2| < b_{\rm qd}$ (light brown) defined in terms of the relative coordinate are indicated.

the height of the peak at $L = 3$, this can be used as a measure of the importance of residual quantum effects in L-changing processes. This is illustrated in Figs. 2(d) and 2(e), which show the probability for remaining in the initial $L = 3$ state as a function of scaled impact parameter, b_0. The quantum simulations [Fig. 2(d)] show that, with increasing b_0, the interaction becomes weaker and this probability increases. In contrast, only small increases are seen in the classical simulations [Fig. 2(e)]. This observation indicates that as b_0 increases quantum effects become increasingly important.

The threshold values $b_{\rm qd,0}$ above which quantum defects suppress L mixing can be approximately estimated from the condition that the peak strength of the dipole field during the collision at the point of closest approach remains below the field strength at which the low-L state crosses the neighboring quasihydrogenic manifold

$$\frac{\langle r\rangle_n}{b_{\rm qd}^3} = \frac{2\delta_L}{3n_{\rm ini}^5}. \tag{11}$$

In Eq. (11), we have estimated the order of magnitude of the dipole moment by the radial size of the n shell, $\langle r\rangle_n$. Equation (11) implies a critical scaled impact parameter

$$b_{\rm qd,0} = \left(\frac{9n_{\rm ini}}{4\delta_L}\right)^{1/3}. \tag{12}$$

(We note that for the states with $\delta_L > 1$ the principal quantum number $n_{\rm ini}$ should be replaced by the nearest integer $\lfloor n_{\rm eff}\rfloor$ of the effective quantum number $n_{\rm eff} = n_{\rm ini} - \delta_L$ and the quantum defect δ_L by $|n_{\rm eff} - \lfloor n_{\rm eff}\rfloor|$). The threshold value [Eq. (12)] explicitly depends, even though only weakly, on $n_{\rm ini}$, thereby directly manifesting the quantum-defect-induced breakdown of the classical scaling invariance. Equation (12) predicts quite accurately the n dependence of the impact parameter above which the initial $L = 3$ state population observed in the quantum simulation remains unchanged [Fig. 2(d)]. For strontium Rydberg $n\,^1F$ states at the predicted thresholds ($b_{\rm qd,0} \simeq 8.0$ for $n_{\rm ini} = 20$, 8.6 for $n_{\rm ini} = 25$, 9.1 for $n_{\rm ini} = 30$, and 9.7 for $n_{\rm ini} = 35$), $\approx 90\%$ of colliding pairs remain in the initial state. With further increase of $n_{\rm ini}$, the value of $b_{qd,0}$ at which quantum effects become important increases, extending the validity of classical simulations to a wider range of impact parameters [see Fig. 3(a)]. For $n\,^1F_3$ states of strontium with $n \approx 300$, $b_{\rm qd,0} \simeq 19.8$, which is more than a factor of 4 larger than the "hard sphere" impact parameter.

For $b_0 < b_{\rm qd,0}$, the cross sections for L changing can be accurately predicted by CTMC simulations. Its approximate size, however, can also be analytically estimated. In this regime, quantum-defect-induced subshell splittings can be neglected and the Stark manifold can be treated as fully degenerate. Accordingly, L changing results from collisionally induced Stark precession. The corresponding precession angle Θ is given by [28,29]

$$\Theta = \int_{-\infty}^{\infty} \omega_F(t)\,dt = \int_{-\infty}^{\infty} \frac{3}{2} n_{\rm ini} F_{\rm eff}(t)\,dt = \frac{9}{2b_0^2 v_{\rm coll,0}}, \tag{13}$$

where $\omega_F(t) = (3/2)n_{\rm ini}F_{\rm eff}(t)$ is the time-dependent Stark precession frequency. Estimating a precession angle of $\simeq \pi/2$ as the threshold for Stark mixing, significant L changing will occur for all $b_0 < b_{S,0}$ with

$$b_{S,0} = \frac{3}{\sqrt{\pi\, v_{\rm coll,0}}}. \tag{14}$$

Note that $b_{S,0}$ is, unlike Eq. (12), fully scaling invariant, i.e., is independent of $n_{\rm ini}$, as expected in an effectively hydrogenic system. Combining the results for dynamical Stark mixing and for its suppression by the quantum defect, the scaled cross

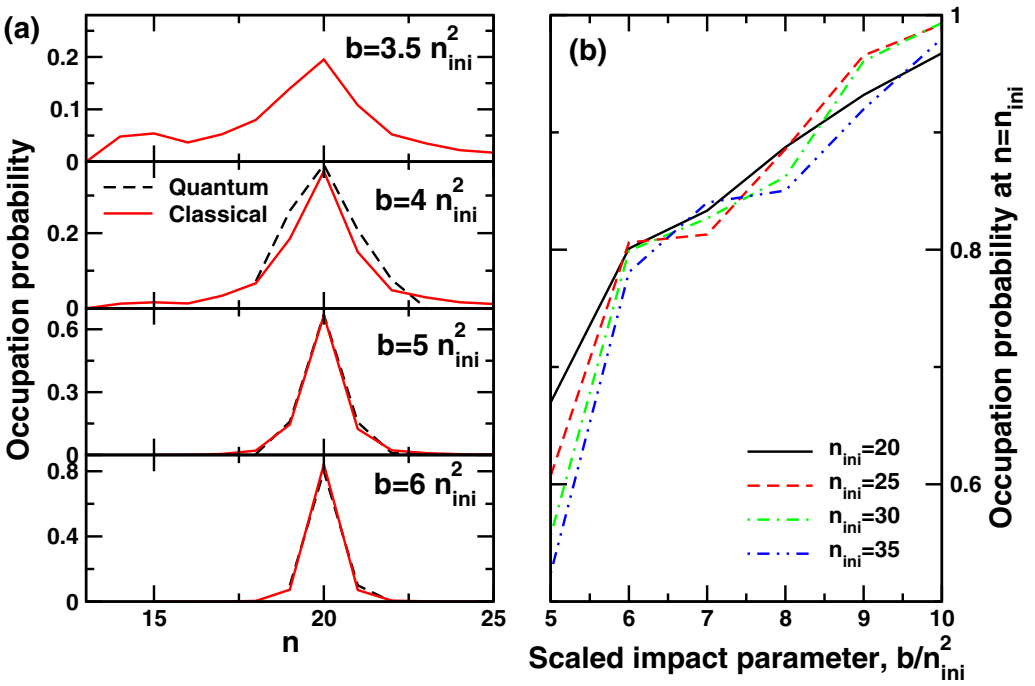

FIG. 4. (a) Final n distributions after a collision between two $L = 3$ Rydberg atoms with $n_{\rm ini} = 20$ for scaled velocity $v_{\rm coll,0} = 0.025$ and the indicated values of impact parameter. The dashed lines show the results of quantum calculations, and the solid lines show those of CTMC simulations. (b) Quantum calculations of the probability for remaining in the initial $n = n_{\rm ini}$ state after collision as a function of the scaled impact parameter for the values of $n_{\rm ini}$ listed.

section for L changing is of the order of

$$\sigma_{L,0}(v_{\rm coll,0}) = \pi \min\left(b_{S,0}^2, b_{\rm qd,0}^2\right). \tag{15}$$

For $n_{\rm ini} = 30$ and a scaled velocity $v_{\rm coll,0} = 0.025$, which corresponds to a thermal collision at $T \simeq 83000\,{\rm K}$, $b_{S,0} = 10.7$ is close to $b_{\rm qd,0} = 9.2$, resulting in a cross section $\sigma_L = n_{\rm ini}^4 \sigma_{L,0} = 265.9 n_{\rm ini}^4 = 2.2 \times 10^8$ (a.u.). Extrapolating to $n_{\rm ini} = 300$, while still using $v_0 = 0.025$ (corresponding to $T \simeq 830\,{\rm K}$), quantum effects first become important for values of $b_{\rm qd,0} = 19.8$ (or $94\,\mu$m) while classical suppression begins for values of $b_{S,0} = 10.7$ (or $51\,\mu$m) [Fig. 3(a)]. Therefore, L changing can be expected for impact parameters as large as $50\,\mu$m corresponding to a giant cross section $\sigma_L \simeq 8 \times 10^{-5}$ cm^2. It should be noted that according to Eq. (15) the size of the quantum defects limits the size of the cross section only if $b_{\rm qd} < b_S$. Therefore, high-n $^1P_1$ Rydberg states, despite their large quantum defect ($\delta_P = 2.73$), should feature similarly large L-changing cross sections controlled by b_S as $b_{\rm qd,0} = 13.6$ for $n_{\rm ini} = 300$ remains above $b_{S,0}$. Only for lower $n_{\rm ini}$ is the cross section delimited by the size of the quantum defect. The crossover $b_{\rm qd} = b_S$ occurs for P states near $n_{\rm ini} = 225$ and near $n_{\rm ini} = 150$ for F states. For $^1F_3$ states and a smaller scaled velocity $v_{\rm coll,0} \approx 7.3 \times 10^{-3}$, which corresponds to a thermal collision of $T = 70.8\,{\rm K}$ at $n_{\rm ini} = 300$, the threshold for Stark mixing $b_{S,0}$ approaches the threshold $b_{\rm qd,0} = 19.8$ for quantum suppression, yielding in this case an upper bound for σ_L of 2.8×10^{-4} cm^2. For such large n, CTMC simulations should provide an accurate prediction of the final L distribution. Such large cross sections can be probed by the present experiment as the critical impact parameter for L-changing at $n_{\rm ini} = 300$ is $b_S = 50\,\mu$m and, thus, comparable to the linear dimension of the excitation volume ($50 \times 70\,\mu$m). [See Fig. 3(b) for the relation between the size of the excitation region and the impact parameter]. Consequently, as two Rydberg atoms within the excitation volume pass by each other, L-changing occurs with near unit probability. We will later test this prediction by comparison with the experiment. For measurements with larger excitation volumes and higher laser powers, tests of these predictions for even higher $n_{\rm ini}(>300)$ would become possible.

Similar analytical estimates can also be made for n-mixing cross sections. The mixing of adjacent n levels requires peak field strengths greater than $F_n = 1/(3n^5)$ at which the most red-shifted Stark state with principal quantum number n and the most blue-shifted Stark state with $n-1$ cross. Such a peak field strength is reached for scaled impact parameter $b_0 < b_{n,0} = (9n_{\rm ini}/2)^{1/3}$. The threshold values of $b_{n,0}$ are 4.5 for $n_{\rm ini} = 20$ and 11.1 for $n_{\rm ini} = 300$ and are well below the thresholds for the suppression of L mixing due to quantum defects. The numerically calculated n distributions following collisions with different impact parameters b_0 (see Fig. 4) show little n mixing for $b_0 = 5$ while for the smaller impact parameter, $b_0 = 4 \simeq b_{n,0}$, population transfer to the neighboring $n = n_{\rm ini} \pm 1$ states becomes significant. Under these conditions, the product n distribution obtained by solving the Schrödinger equation is well approximated by the CTMC simulations. This results because the probability to be in a particular n level is obtained by integration over a noninteger range of classical actions between $n - 1/2 < n_{\rm cl} < n + 1/2$, which averages out the effect of the quantum defect. At an even smaller impact parameter $b_0 = 3.5$, the effective field $F_{\rm eff}$ changes more rapidly as the atoms pass by each other and the likelihood of transitions to the continuum increases. Consequently, collisions can lead to excitation to very high-n

states or to ionization in which one of the collision partners is de-excited to a lower n level. This is apparent in the CTMC simulations, which yield an n-distribution peaked at $n = n_{\rm ini}$ but with a long tail extending into the high-n regime (and above the ionization threshold) and an additional small but noticeable peak around $n \lesssim n_{\rm ini}/\sqrt{2}$ [Fig. 4(a)]. This latter peak mirrors the high density of states in the vicinity of the ionization threshold. Given the broad range of accessible final states, it is not possible to obtain converged results using the current quantum simulations and a limited set of basis states that includes only bound states with $14 \leqslant n \leqslant 23$. Additionally, at small b_0, the higher order interaction terms beyond $V_{\rm dd}$ become non-negligible. However, any ionized atoms are discriminated against in the present pump-probe measurements. Furthermore, the ionizing fields used for SFI are such that any product atoms with $n \lesssim n_{\rm ini}/\sqrt{2}$ ($\simeq 210$ for $n_{\rm ini} = 300$) are not detected. For large impact parameters $b > b_n$, the fraction of the atoms that remain in the parent $n_{\rm ini}$ level is nearly independent of $n_{\rm ini}$ [see Fig. 4(b)] which is consistent with classical scaling invariance and further supports use of classical simulations for atoms undergoing n-changing processes with small Δn. We note that good agreement between the classical and quantum simulations is obtained only when the model potential in Eq. (6) is used in the classical simulations. For a pure Coulomb potential n-changing processes are strongly suppressed in the CTMC simulations.

V. SIMULATION OF THE PUMP-PROBE MEASUREMENT

For a quantitative comparison between the theoretical predictions for L changing in Rydberg-Rydberg collisions discussed above and experimental data, the results of the microscopic description of the electron dynamics during the collision are used as input to a mesoscopic simulation of scattering of an ensemble of atoms in a thermal atomic beam. The distribution of relative velocities $v_{\rm coll}$ and impact parameters b for the Rydberg atoms formed in a hot atomic beam are required to model the thermal averages of the (n, L) distributions that will result from collisions between two Rydberg atoms. Such averaged distributions will, in turn, serve as the input to the simulation of the subsequent pump-probe sequence employed in the measurement.

The population of excited Rydberg atoms in the excitation volume and beyond accounting for blockade effects is described by a set of rate equations [26,31] which we solve by a Monte Carlo algorithm. This Monte Carlo method should not be confused with the CTMC approach to the microscopic electronic dynamics in a binary Rydberg-Rydberg collision discussed above. Once an ensemble of Rydberg atoms is created, the distribution of b and $v_{\rm coll}$ is determined. The simulations of the current experimental setup indicate that more than 90% of Rydberg atom pairs have an impact parameter below $b_{S,0} = 10.7$ (or 51 μm) and for about 33% the impact parameter lies within the range $30\,\mu{\rm m} < b < 51\,\mu{\rm m}$. Thus, given the large predicted cross sections, the effects of L-changing interactions should be readily apparent. The final (L, n) distribution after collisions follows from convolution of the b and $v_{\rm coll}$ distributions with the probability distribution for L changing [Eq. (9)] discussed in Sec. IV. As a typical example, we show in Fig. 5 the calculated (L, n) distribution, P_{nL}, following a 6-μs-duration laser excitation pulse. Of the parent Rydberg atoms, $\approx 34\%$ remain in the initial $n_{\rm ini} = 297$, $L = 3$ state. Those Rydberg atoms that undergo collisions have a broad distribution of final L states ranging from 0 to the maximum value $n - 1$ and high-L states ($L > 100$) are mainly populated. The n distribution remains centered on $n = n_{\rm ini}$ but is slightly broadened.

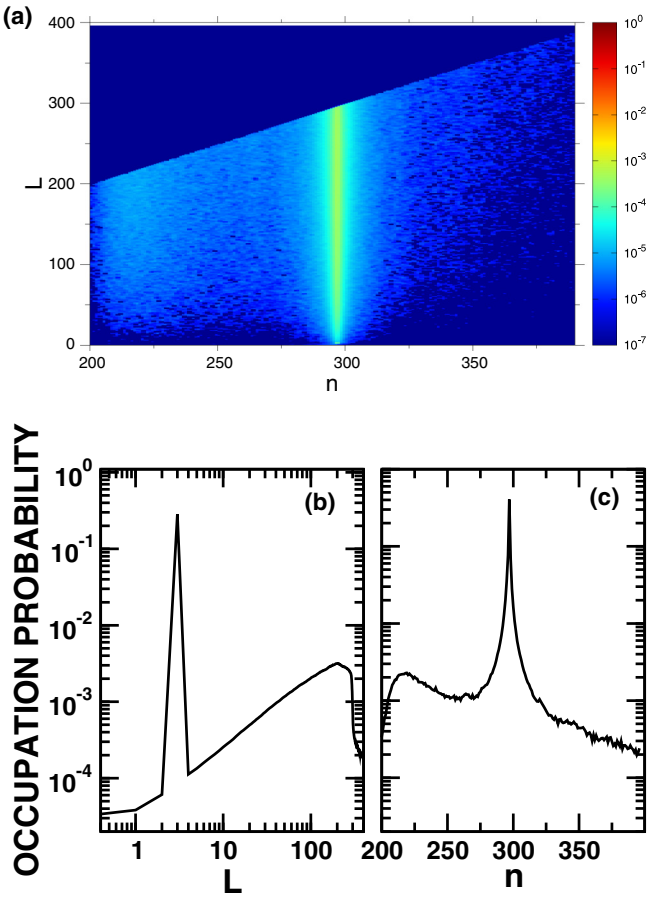

FIG. 5. (a) Calculated (L, n) distribution of Rydberg atoms following excitation by a 6-μs-long laser pulse with power sufficient to create $\langle N_{\rm Ryd}\rangle \approx 15$ Rydberg atoms. [(b), (c)] Reduced L and n distributions obtained by integrating the distributions in panel (a) over n or L.

In the experiment, the distribution of product states formed through collisions is monitored by a pump-probe pulse sequence. The pump pulse consists of the sudden turn-on of a constant electric field $F_{\rm pump}$. While this electric field also induces Stark precession [to be distinguished from collisionally induced precession (see below)], the short rise time triggers nonadiabatic transitions, which broaden the n distribution. Consequently, the resulting coherent superposition of n levels forms a wave packet evolving with the Kepler frequency $\nu_K = (E_n - E_{n-1})/(2\pi) \simeq 1/(2\pi n^3)$. In the current experimental setup, $F_{\rm pump}$ is much larger than the effective field $F_{\rm eff}$ induced by collisions and the pulse duration is short (≈ 400 ns). Therefore, while the pump field is applied, Stark precession is dominated by the pump pulse and is largely unaffected by collisions. The probe pulse is about 600 ps long,

much shorter than the inverse Kepler frequency ν_K^{-1}, i.e., the classical orbital period of the Rydberg electron, ≈ 4 ns for $n_{\rm ini} \approx 300$. Therefore, by varying the time delay between the application of the pump and the probe pulses both the slow Stark precession and fast Kepler motion can be resolved. The probe pulse $\vec{F}_{\rm probe}(t)$, polarized along the z axis, delivers a momentum transfer $\Delta p\hat{z} = -\int_{-\infty}^{\infty} \vec{F}_{\rm probe}(t)dt$ to the excited electron. In the impulsive limit [i.e., $\vec{F}_{\rm probe}(t) = -\Delta p\hat{z}\delta(t)$], the probe pulse transfers energy $\Delta E = \Delta p^2/2 + p_{z_i}\Delta p$ to the Rydberg electron that depends on its initial z component of momentum, p_{z_i}. By choosing $\Delta p \sim -1/n_{\rm ini}$, electrons with negative p_{z_i} are ionized while those with positive p_{z_i} remain bound. Therefore, for stationary states, which provide a convenient reference, $\approx 50\%$ of the atoms will be ionized. For a finite-duration probe pulse, the kick strength Δp also needs to be adjusted to obtain an ionization probability of about 50%. For wave packets generated by the pump pulse, the survival probability will oscillate around this value displaying "quantum" beats due to both n mixing (Kepler beats) and L mixing (Stark beats). While the angular momentum $\vec{L}$ evolves with the frequency $\nu_F = \omega_F/(2\pi)$, the ionization probability depends only on the magnitude L (or, more precisely, its square L^2) and, therefore, evolves with the frequency $\nu_S = 2\nu_F$. The frequency of the Stark quantum beats is typically much smaller than the Kepler frequency.

The information extracted from this pump-probe protocol can be simulated by another microscopic CTMC simulation [30] treating single Rydberg atoms interacting with pump and probe fields rather than Rydberg atom–Rydberg atom interactions. Accordingly, the atomic rather than the molecular Hamilton function [Eqs. (3)–(6)] enters the equations of motion and the initial phase-space distribution of these simulations corresponds to the electronic wave packet in the atom formed by the collision. We first demonstrate that pump-probe sequences of the type just discussed succeed in extracting information on the changes in the n and L distributions induced by collisions. The encoding of the information on the L distribution in the pump-probe signal is illustrated in Fig. 6 which shows the survival probabilities (i.e., one minus the ionization probability) of Rydberg atoms initially with $P_{nL} = \delta_{n,297}\delta_{L,L_i}$ calculated for a 300-ps rise-time pump pulse with $F_{\rm pump} = 9.3$ mV/cm and a 600-ps probe pulse with $\Delta p = -0.85/n_{\rm ini}$ for several initial angular momenta L_i [Figs. 6(a)–6(d)]. The orientation of $\vec{L}_i$ (i.e., the magnetic quantum number M) is randomly distributed. The low-frequency oscillations correspond to Stark precession ($\nu_S \simeq 10$ MHz) and the fast oscillations to Kepler beats ($\nu_k \simeq 250$ MHz). Figures 6(e)–6(h) show the modulus of the Fourier amplitudes, $|f(\nu)|$, of the survival probabilities and reveal the additional presence of higher harmonics of the Stark frequency. Moreover, the peak associated with the Kepler beats is split into two peaks with frequencies $\nu_K \pm \nu_F$ separated by $\nu_S = 2\nu_F$ (indicated by arrows). Quantum mechanically, the dipole matrix elements $\langle n', k', m|z|n, k, m\rangle$ [43] decay rapidly with increasing $n - n'$ and $|k - k'|$. Therefore, the expectation value $\langle z(t)\rangle$ is dominated by a superposition of states coupled by the dipole matrix elements with $n' = n \pm 1$ and $k' = k \pm 1$ which evolve with frequencies $\nu_K \pm \nu_F$. Classically, the Stark frequencies $\nu_k \pm \nu_F$ appear in the Fourier spectrum of trajectories whose

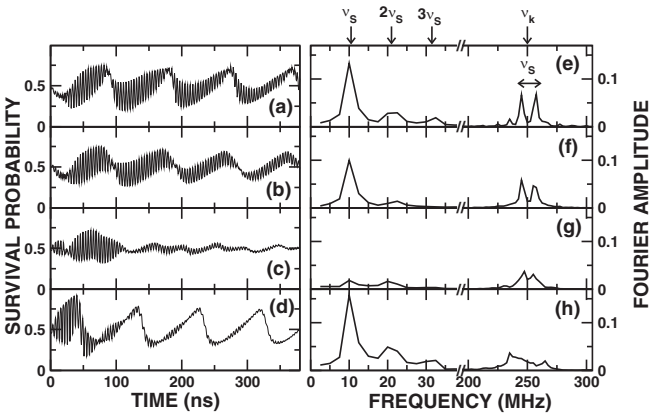

FIG. 6. [(a)–(d)] Calculated survival probabilities and [(e)–(h)] their Fourier amplitudes $|f(\nu)|$ for a Rydberg atom with $n_{\rm ini} = 297$ subject to a pump pulse $F_{\rm pump} = 9.3$ mV/cm and a probe pulse with $\Delta p = -0.85/n_{\rm ini}$. The initial angular momentum is [(a), (e)] $L = 3$; [(b), (f)] 100; [(c), (g)] 200; and [(d), (h)] 296. The magnetic quantum number M is randomly distributed in the range $-L \leqslant M \leqslant L$.

Runge-Lenz vectors are aligned parallel or antiparallel to the pump field. The dependence of the amplitudes and damping of these beats on the angular momenta involved can be analyzed by frequency filtering (see Fig. 7). For initial angular momenta $L_i = 3$ and $L_i = 100$, the Fourier amplitudes [Figs. 6(e) and 6(f)], display a Stark split Kepler frequency component $\nu = \nu_k \pm \nu_F$. Resolution of this frequency splitting is consistent with the slow damping of the Kepler beats [see Figs. 7(a) and 7(b)]. For $L_i = 200$ and 296, these two peaks coalesce to one broad peak with width $\delta\nu \simeq \nu_S$ [see Figs. 6(g) and 6(h)]. Correspondingly, the Kepler beats are quickly damped on a timescale of $\approx 1/\nu_S \simeq 100$ ns. In contrast, the Stark

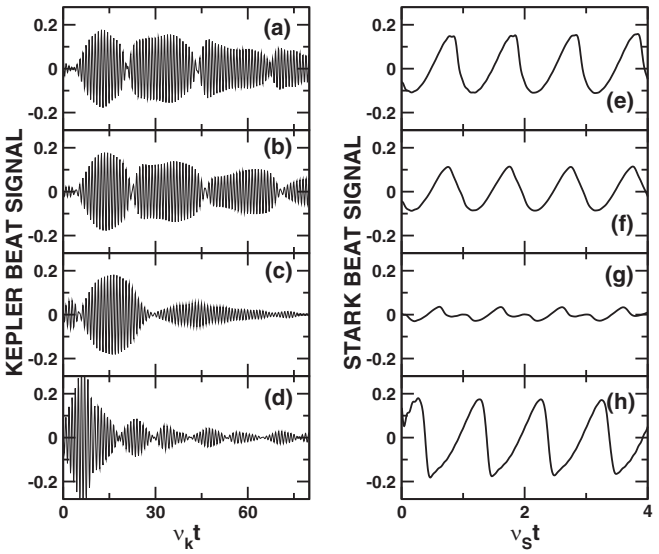

FIG. 7. Frequency-filtered quantum beat signals. [(a)–(d)] High- and [(e)–(h)] low-frequency components of the survival probabilities in Figs. 6(a) to 6(d) obtained by taking the inverse Fourier transform of $f(\nu)$ within frequency windows of [(a)–(d)] 200 to 300 MHz and [(e)–(h)] 2.5 to 120 MHz.

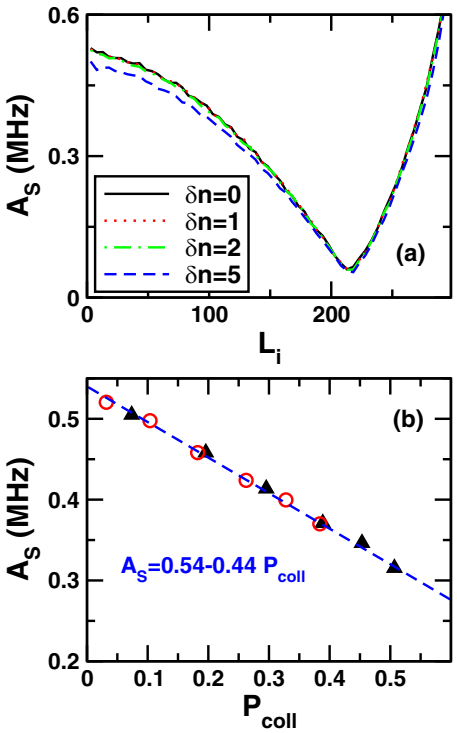

FIG. 8. (a) Integrated area A_S under the peak around the Stark frequency ν_S in the Fourier amplitude of the survival probability (see Fig. 6). The initial state is approximated by ensembles of trajectories with principal action following a Gaussian distribution centered at $n_{\rm ini} = 297$ with a standard deviation δn varying between 0 and 5. (b) Stark beat strength A_S as a function of the collision probability $P_{\rm coll}$ that a Rydberg atom traverses at least another Rydberg atom during the excitation laser pulse. The laser power is adjusted to excite $\langle N_{\rm Ryd}\rangle \approx 8$ atoms (triangles) or ≈ 5 atoms (circles) in 3 μs and the Stark beats are probed at $t = 0.5, 1, 1.5, 2, 2.5, 3$ μs. The pump field and probe impulse are set to $F_{\rm pump} = 9.3$ mV/cm and $\Delta p = -0.85/n_{\rm ini}$, respectively.

beat signals [Figs. 7(e)–7(h)] on which we will focus in the following do not show any sign of significant damping within 400 ns (the typical timescale used in the experiments). Their overall amplitudes, however, depend markedly on L_i. The beat amplitudes decrease with increasing L_i up to a local minimum near $L_i \simeq 200$, after which the amplitudes rise again but are accompanied by a π phase shift.

The beat strength can be quantified by the integrated Fourier amplitude

$$A_S = \int_{(1/2)\nu_S}^{(3/2)\nu_S} |f(\nu)| d\nu. \tag{16}$$

A_S exhibits a strong L_i dependence with a minimum around $L_i \simeq 200$ [see Fig. 8(a)]. This minimum at the intermediate values of L_i results from two competing trends. For initial angular momenta at both ends of the L spectrum, i.e., $L_i \simeq 0$ and $L_i \simeq n-1 \simeq 300$, Stark mixing leads to a rapid increase (or decrease) of L within the classical ensemble resulting in Stark beats with large amplitude A_S. For intermediate initial $L_i \simeq 210$ corresponding to $L_i^2 \simeq n^2/2$, the classical ensemble contains subensembles of trajectories of similar weights for which the Stark precession leads to either an increase or a decrease of L. Even when the n distribution is broadened, i.e., $P_{nL} \propto \delta_{L,L_i} \exp(-(n-n_{\rm ini})^2/[2(\delta n)^2])$ [Fig. 8(a)], the small changes $3\delta n F_{\rm pump}$ induce little dephasing in the Stark beats and the beat strength A_S is reduced only slightly with increasing δn. This demonstrates that A_S provides a good measure for L-changing processes even when the n distribution is broadened. Since the initial Rydberg state with $L_i = 3$ yields a large Stark beat amplitude, any reduction in A_S indicates a change in L or a broadening in the L distribution P_{nL}. Indeed, as seen in Fig. 8(b), the Stark beat strength A_S decreases steadily with increasing collision probability $P_{\rm coll}$ for a Rydberg atom to pass by another Rydberg atom. In practice, the collision probability is determined within the Monte Carlo simulation of the collisional interaction in the thermal atomic beam by recording the number of Rydberg atoms passing by another Rydberg atom (i.e., reaching the minimum distance $R = b$) within the duration of excitation laser. The probability of an L-changing collision, $P_{\rm coll,L}$, is proportional to this collision probability, i.e., $P_{\rm coll,L} = O_L P_{\rm coll}$, where O_L is the fraction of the atoms in the excitation volume for which the impact parameter for Rydberg-Rydberg collision is $b < b_S$ [see Fig. 3(b)]. Accordingly, O_L is a measure for the L-changing cross section. With increasing pulse duration, $\langle N_{\rm Ryd}\rangle$ increases and so does $P_{\rm coll}$. When $P_{\rm coll}$ approaches unity and simultaneously A_S is strongly damped, nearly all Rydberg atoms must undergo L-changing collision, i.e., $O_L \simeq 1$. Consequently, $A_S \simeq 0$ at $P_{\rm coll} \simeq 1$ is a clear signature that the cross section σ_L is as large as $\pi R_{\rm ex}^2$, where $R_{\rm ex}$ is the linear dimension of the excitation volume [Fig. 3(b)]. On the other hand, when b_S is smaller than a linear dimension of the excitation volume, the Stark beat strength will remain finite even in the limit of $P_{\rm coll} = 1$ from which the value of O_L can be extracted. By extrapolating to $P_{\rm coll} = 1$, the simulation [Fig. 8(b)] yields $A_S \simeq 0.1$, indicating that the L-changing cross section is comparable to the excitation region (50×70 μm). Indeed, a detailed analysis of the simulation gives $O_L \simeq 90$–96%, consistent with a linear dimension of 70 μm of the excitation volume slightly larger than $b_S \simeq 50$ μm. This method will be used later to extract the L-changing cross section from the experimental data. We note that, though A_S is large at $L \simeq 0$ and $n-1$ [Fig. 8(b)], a broadening of the L distribution results in a suppression of A_S. This is due to the destructive interference of Stark beats which oscillate with the opposite phase for $L \simeq 0$ and $n-1$ (Fig. 6).

VI. RESULTS

For the experimental results presented in the following, the amplitudes of the pump pulses used to generate the pump fields were selected to generate steady-state fields of 9.3 mV cm^{-1} (see below). The magnitude of the probe pulse was adjusted to achieve an average survival probability of $\approx 50\%$ to maximize the amplitudes of the quantum beat oscillations. Results were recorded for collisions involving two $5s297f\ ^1F_3$ Rydberg atoms. To identify the effect of collisions on the quantum beats, the number of Rydberg atoms $\langle N_{\rm Ryd}\rangle$ generated by the laser pulse was varied, either by keeping the duration of the laser pulse fixed (3 μs) while varying the

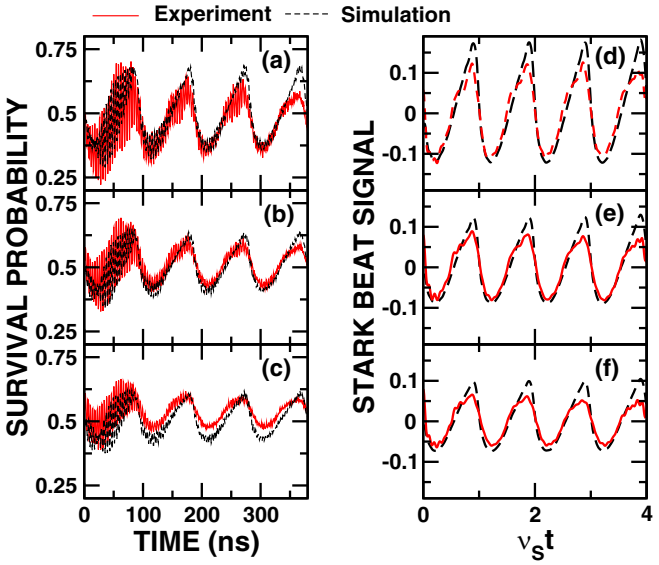

FIG. 9. Measured survival probabilities as a function of the time delay between application of the pump and probe fields. The results were recorded using $5s297f\ ^1F_3$ Rydberg atoms and a fixed 3-μs-long laser pulse with the laser powers adjusted to obtain average numbers of excited Rydberg atoms of (a) $\langle N_{\rm Ryd}\rangle = 1$, (b) 5.7, and (c) 8.3. The (steady-state) pump field is 9.3 mV cm^{-1} and the probe pulse delivers an impulse $\Delta p \approx -0.85/n_{\rm ini}$. [(d)–(f)] the Stark beats associated with each data set after frequency filtering. The simulations assume a probe impulse $\Delta p = -0.85/n_{\rm ini}$ and that application of the pump field leads to a distribution of n with $\delta n = 1$.

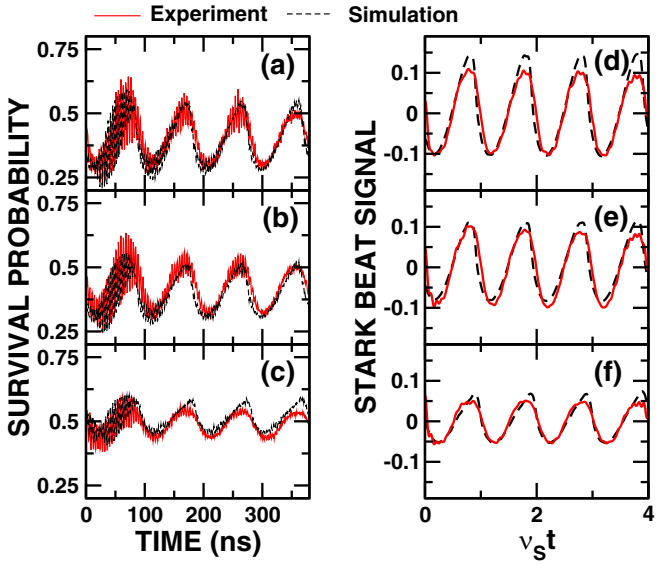

FIG. 10. Survival probabilities measured using $5s297f\ ^1F_3$ Rydberg atoms as a function of the time delay between application of the pump and probe fields for laser pulse widths of [(a), (b)] 1.5 and (c) 6 μs, with the laser powers adjusted to excite average numbers of Rydberg atoms $\langle N_{\rm Ryd}\rangle$ (a) 0.7, (b) 4, and (c) 15. The (steady-state) pump field is 9.3 mV cm^{-1} and the probe impulse is $\Delta p \approx -0.85/n_{\rm ini}$. [(d)–(f)] The Stark beats associated with each data set after frequency filtering. The simulations assume $\delta n = 1$.

laser power (Fig. 9) or by keeping the laser power fixed while varying the duration of the laser pulse (Fig. 10).

Figure 9 shows results obtained using a 3-μs-duration laser pulse with the laser powers adjusted to create different numbers of Rydberg atoms. Values of $\langle N_{\rm Ryd}\rangle$ of 1 [Fig. 9(a)], 5.7 [Fig. 9(b)], and 8.3 [Fig. 9(c)] were selected and result in collision probabilities of $P_{\rm coll} \approx 8\%$, $\approx 38\%$, and $\approx 51\%$, respectively. (The pump and probe fields for all these measurements are identical). At the lowest laser power (i.e., $\langle N_{\rm Ryd}\rangle \sim 1$), the effects of collisions are negligible. These data thus serve as the reference for identifying changes in the quantum beat signal that result from collisions. As the probability for collisions increases, the strength of Stark beats, i.e., A_S, decreases from $A_S = 0.3$ for $\langle N_{\rm Ryd}\rangle \simeq 1$ to $A_S = 0.22$ for $\langle N_{\rm Ryd}\rangle \simeq 5.7$, and to $A_S = 0.17$ for $\langle N_{\rm Ryd}\rangle \simeq 8.3$. Figure 9 also includes the results of the simulations which include a broadening of the n distribution with $\delta n = 1$ induced by small overshoots and ringing in the pump and probe pulses. The beat amplitudes are slightly overestimated by the simulations but the systematic reduction due to collisions is well reproduced.

As shown in Fig. 10, additional evidence for the role of collisions in state changing can be obtained using different laser pulse durations, 1.5 and 6 μs. When using 1.5-μs-long laser pulses, the laser powers were adjusted to produce ≈ 1 and ≈ 4 Rydberg atoms per pulse. Even at the higher laser power, the likelihood that, once created, an atom will suffer a collision is small (the estimated collision probability is $P_{\rm coll} \approx 28\%$). In consequence, only a small reduction in the quantum beat amplitudes is expected, which is consistent with the observed $\approx 10\%$ reduction in A_S [see Figs. 10(a), 10(b) 10(d), and 10(e)]. The situation is rather different when using a 6-μs-long laser pulse. At the highest laser power, ≈ 15 Rydberg atoms can be produced per pulse. Even though the laser powers used to generate the results in Figs. 10(b) and 10(c) are nearly the same, the probability for undergoing a collision increases from $P_{\rm coll} \simeq 28\%$ (for $\langle N_{\rm Ryd}\rangle \simeq 4$) to 66% (for $\langle N_{\rm Ryd}\rangle \simeq 15$). In the latter case, A_S [Figs. 10(c)–10(f)] is reduced by $\approx 50\%$, clearly demonstrating the damping of beats by collisions. The simulations reproduce the observed reduction in A_S very well, providing direct evidence of strong collision-induced L changing.

In order to extract direct information on the L-changing cross section, the measured Stark beat strength A_S is plotted as a function of collision probability $P_{\rm coll}$ (Fig. 11). Because of the n broadening induced by the pump-probe measurement, the Stark beat strength in the absence of collisions is, in general, smaller than that seen in Fig. 8(b). Nevertheless, we observe a similar decrease of A_S with increase of $P_{\rm coll}$, clearly confirming collisional decoherence as the origin of the attenuation of the Stark beats. Extrapolating now the fitted function $A_S(P_{\rm coll})$ to $P_{\rm coll} = 1$ yields a near zero beat amplitude $A_S \simeq 0.05$. This result confirms that the threshold value b_S is comparable to the linear dimension of the excitation region ($50 \times 70\ \mu$m), i.e., the size of of cross section σ_L for L changing is, indeed, of the order of $\sigma_L \simeq 8 \times 10^{-5}$ cm^2.

A limited set of measurements were also performed using $^1P_1$ Rydberg states. Although the photoexcitation rates for P states are substantially smaller than than those for F states, by use of longer laser pulses a sufficient number of $^1P_1$ atoms could be generated to observe effects of their collisions. Direct

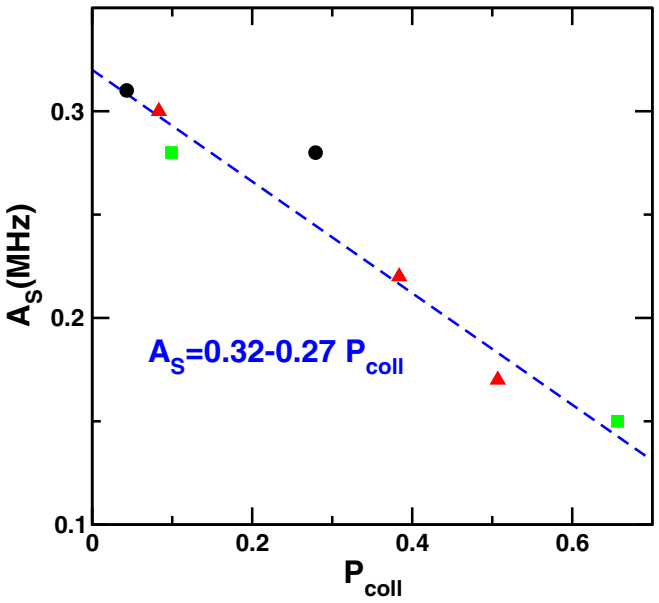

FIG. 11. Stark beat strength A_S as a function of the collision probability $P_{\rm coll}$ that a Rydberg atom traverses at least another Rydberg atom during the excitation laser pulse. $P_{\rm coll}$ is estimated from the pulse duration and $\langle N_{\rm Ryd}\rangle$. A_S is evaluated from the pump-probe signals of Figs. 9(d)–9(f) (triangles), Figs. 10(d) and 10(e) (circles), and Fig. 10(f) (squares).

comparison between data recorded, under identical experimental conditions, with the laser powers adjusted to create equal numbers of P and F states revealed that for both species collisions resulted in similarly strong damping of the Stark quantum beat amplitudes, indicating that the cross sections for L changing in collisions between P states are as large as those for collisions between F states. This is consistent with the theoretical prediction, noted earlier, that for both species the L-changing cross section is limited by classical effects, i.e., by the value of $b_{S,0}$, and not by their quantum defects, which are significantly different.

VII. CONCLUSIONS

The present study demonstrates that long-range interactions during thermal-energy collisions between very-high-n, $n \approx 300$ $n\,^1F_3$, Rydberg atoms can lead to rapid state changing. Simulations show that thermal collisions at $T \approx 830$ K can lead to strong L mixing, even for impact parameters as large as $\approx 50\,\mu$m. The corresponding cross sections, $\approx 8 \times 10^{-5}$ cm^2, are big and significantly larger than those typically associated with neutral-neutral collisions, a prediction that is confirmed by experiment. Extrapolation to lower n and colder collisions suggest that the cross section for L changing increases by another factor of ≈ 4. In consequence, the possibility of state-changing interactions must be considered whenever Rydberg-Rydberg interactions are utilized to probe the behavior of few- and many-body systems. The present work also demonstrates that measurements of quantum beats generated by sudden application of a pump field can provide a valuable complement to selective field ionization when investigating L-changing reactions.

ACKNOWLEDGMENTS

Research has been supported by the NSF under Grants No. 1600059 and No. 1904294, the Robert A. Welch Foundation under Grant No. C-0734, the FWF (Austria) Grants No. FWF-SFB041ViCom and No. FWF-Doctoral College W1243. The Vienna Scientific Cluster was used for the calculations.

[1] F. Maucher, N. Henkel, M. Saffman, W. Królikowski, S. Skupin, and T. Pohl, Phys. Rev. Lett. **106**, 170401 (2011).
[2] N. Henkel, R. Nath, and T. Pohl, Phys. Rev. Lett. **104**, 195302 (2010).
[3] M. Boninsegni and N. V. Prokof'ev, Rev. Mod. Phys. **84**, 759 (2012).
[4] B. Yan, S. A. Moses, B. Gadway, J. P. Covey, K. R. A. Hazzard, A. M. Rey, D. S. Jin, and J. Ye, Nature (London) **501**, 521 (2013).
[5] K. R. A. Hazzard, B. Gadway, M. Foss-Feig, B. Yan, S. A. Moses, J. P. Covey, N. Y. Yao, M. D. Lukin, J. Ye, D. S. Jin *et al.*, Phys. Rev. Lett. **113**, 195302 (2014).
[6] A. de Paz, A. Sharma, A. Chotia, E. Maréchal, J. H. Huckans, P. Pedri, L. Santos, O. Gorceix, L. Vernac, and B. Laburthe-Tolra, Phys. Rev. Lett. **111**, 185305 (2013).
[7] G. Pupillo, A. Micheli, M. Boninsegni, I. Lesanovsky, and P. Zoller, Phys. Rev. Lett. **104**, 223002 (2010).
[8] Y.-Y. Jau, A. M. Hankin, T. Keating, I. H. Deutsch, and G. W. Biedermann, Nat. Phys. **12**, 71 (2015).
[9] T. Amthor, M. Reetz-Lamour, S. Westermann, J. Denskat, and M. Weidemüller, Phys. Rev. Lett. **98**, 023004 (2007).
[10] D. Tong, S. M. Farooqi, J. Stanojevic, S. Krishnan, Y. P. Zhang, R. Côté, E. E. Eyler, and P. L. Gould, Phys. Rev. Lett. **93**, 063001 (2004).
[11] K. Singer, M. Reetz-Lamour, T. Amthor, L. G. Marcassa, and M. Weidemuller, Phys. Rev. Lett. **93**, 163001 (2004).
[12] E. Urban, T. A. Johnson, T. Henage, L. Isenhower, D. D. Yavuz, T. G. Walker, and M. Saffman, Nat. Phys. **5**, 110 (2009).
[13] A. M. Hankin, Y.-Y. Jau, L. P. Parazzoli, C. W. Chou, D. J. Armstrong, A. J. Landahl, and G. W. Biedermann, Phys. Rev. A **89**, 033416 (2014).
[14] D. Barredo, S. Ravets, H. Labuhn, L. Béguin, A. Vernier, F. Nogrette, T. Lahaye, and A. Browaeys, Phys. Rev. Lett. **112**, 183002 (2014).
[15] J. Deiglmayr, Phys. Scr. **91**, 104007 (2016).
[16] M. Ciocca, M. Allegrini, E. Arimondo, C. E. Burkhardt, W. P. Garver, and J. J. Leventhal, Phys. Rev. Lett. **56**, 704 (1986).
[17] T. F. Gallagher, K. A. Safinya, F. Gounand, J. F. Delpech, W. Sandner, and R. Kachru, Phys. Rev. A **25**, 1905 (1982).
[18] E. Fiordilino, G. Ferrante, and B. M. Smirnov, Phys. Rev. A **35**, 3674 (1987).
[19] A. N. Klyucharev, N. N. Bezuglov, A. A. Mihajlov, and L. M. Ignjatović, J. Phys.: Conf. Ser. **257**, 012027 (2010).

[20] W. Li, P. J. Tanner, and T. F. Gallagher, Phys. Rev. Lett. **94**, 173001 (2005).
[21] T. Amthor, M. Reetz-Lamour, C. Giese, and M. Weidemüller, Phys. Rev. A **76**, 054702 (2007).
[22] K. R. Overstreet, A. Schwettmann, J. Tallant, and J. P. Shaffer, Phys. Rev. A **76**, 011403(R) (2007).
[23] M. Viteau, A. Chotia, D. Comparat, D. A. Tate, T. F. Gallagher, and P. Pillet, Phys. Rev. A **78**, 040704(R) (2008).
[24] F. Robicheaux, J. Phys. B **38**, S333 (2005).
[25] Z. Feng, J. Miao, K. Zhao, D. Li, Z. Yang, F. Wu, Z. Wu, J. Zhao, and S. Jia, J. Phys. Soc. Jpn. **85**, 054301 (2016).
[26] G. Fields, F. B. Dunning, S. Yoshida, and J. Burgdörfer, Phys. Rev. A **99**, 022710 (2019).
[27] R. E. Olson, Phys. Rev. Lett. **43**, 126 (1979).
[28] I. C. Percival and D. Richards, J. Phys. B **12**, 2051 (1979).
[29] S. Yoshida, C. O. Reinhold, J. Burgdörfer, W. Zhao, J. J. Mestayer, J. C. Lancaster, and F. B. Dunning, Phys. Rev. A **78**, 063414 (2008).
[30] S. Yoshida, C. O. Reinhold, J. Burgdörfer, W. Zhao, J. J. Mestayer, J. C. Lancaster, and F. B. Dunning, Phys. Rev. A **75**, 013414 (2007).
[31] S. Yoshida, J. Burgdörfer, X. Zhang, and F. B. Dunning, Phys. Rev. A **95**, 042705 (2017).
[32] X. Zhang, F. B. Dunning, S. Yoshida, and J. Burgdörfer, Phys. Rev. A **92**, 051402(R) (2015).
[33] A. Salin, Eur. Phys. J. D **8**, 189 (2000).
[34] C. L. Vaillant, M. P. A. Jones, and R. M. Potvliege, J. Phys. B **45**, 135004 (2012).
[35] C. Bottcher, J. Phys. B **14**, L349 (1981).
[36] N. B. Delone, S. P. Goreslavsky, and V. P. Krainov, J. Phys. B **27**, 4403 (1994).
[37] R. Ding, J. D. Whalen, S. K. Kanungo, T. C. Killian, F. B. Dunning, S. Yoshida, and J. Burgdörfer, Phys. Rev. A **98**, 042505 (2018).
[38] L. Couturier, I. Nosske, F. Hu, C. Tan, C. Qiao, Y. H. Jiang, P. Chen, and M. Weidemüller, Phys. Rev. A **99**, 022503 (2019).
[39] C. Lanczos, J. Res. Natl. Bur. Stand. B **45**, 255 (1950).
[40] T. J. Park and J. C. Light, J. Chem. Phys. **85**, 5870 (1986).
[41] R. Abrines and I. C. Percival, Proc. Phys. Soc. **88**, 861 (1966).
[42] S. Yoshida, C. O. Reinhold, J. Burgdörfer, B. E. Tannian, R. A. Popple, and F. B. Dunning, Phys. Rev. A **58**, 2229 (1998).
[43] H. A. Bethe and E. E. Salpeter, *Quantum Mechanics of One- and Two-Electron Atoms* (Plenum, New York, 1977).